

Porous Coordination Polymer Hybrid Device with Quartz Oscillator: Effect of Crystal Size on Sorption Kinetics


Hiromitsu Uehara,[†] Stéphane Diring,^{†,‡} Shuhei Furukawa,^{*,†,‡} Ziya Kalay,[‡] Manuel Tsotsalas,[‡] Masashi Nakahama,[†] Kenji Hirai,[§] Mio Kondo,[‡] Osami Sakata,^{||} and Susumu Kitagawa^{*,†,‡,§}

[†]ERATO Kitagawa Integrated Pores Project, Japan Science and Technology Agency, Kyoto Research Park Building 3, Shimogyo-ku, Kyoto 600-8815, Japan

[‡]Institute for Integrated Cell-Material Science, Kyoto University, Yoshida, Sakyo-ku, Kyoto 606-8501, Japan

[§]Department of Synthetic Chemistry and Biological Chemistry, Graduate School of Engineering, Kyoto University, Katsura, Nishikyo-ku, Kyoto 615-8510, Japan

^{||}Synchrotron X-ray Laboratory at SPring-8, National Institute for Materials Science, Kouto, Sayo, Hyogo 679-5198, Japan

 Supporting Information

ABSTRACT: A new strategy to synthesize monodispersed porous coordination polymer (PCP) nanocrystals at room temperature was developed and utilized for the formation of PCP thin films on gold substrates with fine control over the crystal sizes using the coordination modulation method. Hybridization of these PCP thin films with an environment-controlled quartz crystal microbalance system allowed determining the adsorption properties for organic vapors (methanol and hexane). In the case of high sensitivity (at the low-concentration dosing of analytes), the sensor response depended on the crystal size but not on the type of analyte. In contrast, at the high-concentration dosing, a clear dependence of the sorption kinetics on the analyte was observed due to significant sorbate–sorbate interaction.

Porous coordination polymers (PCPs), assembled from metal ions and organic bridging ligands, are an intriguing class of porous materials because of their potential applications for gas storage, selective gas separation, and heterogeneous catalysis.^{1–10} Although the nanosized pores of PCPs inherently possess favorable properties for such applications, the hybridization of PCPs with electronic devices promises a great enhancement of chemical sensing performance. In particular, a quartz crystal microbalance (QCM) that converts a change of mass to a change of oscillation frequency is a good candidate for use as a delicate electronic sensor into which PCP crystals can be integrated.^{11,12} Its gravimetric sensing ability allows quantitative analysis of molecular adsorption on the nanogram scale and real-time monitoring of sorption processes.

A lot of efforts have recently been dedicated to finding strategies to control and reduce the size of PCP crystals to the nanoscale,¹³ especially for the fabrication of porous thin films by immobilizing those PCPs on various substrates.¹⁴ When the crystal size is decreased, the length of the diffusion pathway becomes shorter, and thus the concentration-dependent diffusion coefficient should play a crucial role in the permeability of guest molecules into the pores. However, the porous properties

of thin films have been rarely investigated,¹⁵ and especially the effect of crystal size or film thickness has not been discussed so far. Here we present the integration of size-controlled PCP nanocrystals into a QCM device and investigate the impact of the crystal size on the sorption kinetics. The objective of this study is not only to gain insight into sorption kinetics or molecular diffusion but also to contribute to the improvement of sensor response.

We recently reported a methodology to control the size and morphology of PCP nanocrystals, the so-called coordination modulation method.¹⁶ The cubic framework of [Cu₃(btc)₂]_n (btc = benzene-1,3,5-tricarboxylate) was selected because we could successfully control the size of the framework in the nano/micro regimes.¹⁷ Here we modified this method to achieve the size-controlled growth of highly homogeneous [Cu₃(btc)₂]_n nanocrystals on gold-coated QCM substrates at room temperature. A stable mother liquor was obtained by mixing copper acetate, H₃btc, and a large amount of dodecanoic acid as a modulator in butanol. The mixture underwent a short microwave pretreatment (413 K, 5 min), which did not cause the formation of precipitate, followed by immersion of a flame-annealed QCM substrate into the mother liquor. The crystallization of nanosized [Cu₃(btc)₂]_n was induced at room temperature by addition of ethanol as a counter solvent. After standing for >12 h, the substrate was then gently washed with a copious amount of ethanol to remove the monocarboxylic modulator. Interestingly, the crystal size of bulk [Cu₃(btc)₂]_n could be tuned by carefully controlling the volume of ethanol added to the mother liquor. Larger volumes of counter solvent induced a rapid crystallization (turbidity appeared in <1 h) and smaller crystals, while larger crystals with well-defined cubic morphology arose from longer crystallization time (6 h) and smaller volume of ethanol (Figure 1; see also Supporting Information (SI)).

The same crystal size dependency was also observed on the gold substrates by means of atomic force microscopy (AFM). As shown in Figure 2a,b, the nanocrystals prepared from the concentrated mother liquor (concentration of H₃btc, *c* = 31.2 mM, and dilution factor, ethanol/mother liquor, *d* = 1) present cubic shapes of

Received: June 2, 2011

Published: July 06, 2011

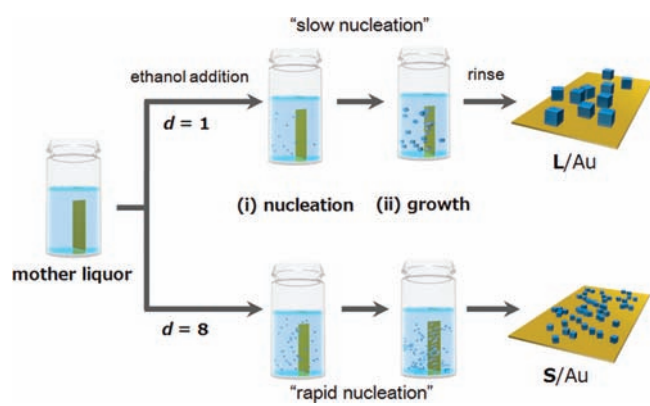


Figure 1. Schematic illustration of size-controlled $[\text{Cu}_3(\text{btc})_2]_n$ nanocrystal formation on gold-coated QCM substrate. d is the dilution factor, ethanol/mother liquor (v/v).

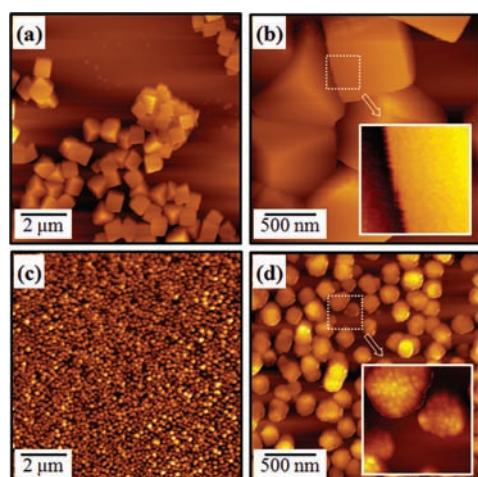


Figure 2. AFM images of $[\text{Cu}_3(\text{btc})_2]_n$ nanocrystals deposited on gold substrate, measured under ambient conditions: (a,b) L/Au and (c,d) S/Au (see text). Scanned areas are (a,c) $10 \times 10 \mu\text{m}^2$ and (b,d) $2 \times 2 \mu\text{m}^2$. (b,d, insets) Enlarged images of the boxed areas ($300 \times 300 \text{nm}^2$).

$614 \pm 11 \text{ nm}$ size (denoted as L/Au). On the other hand, the highly diluted solution ($c = 7.9 \text{ mM}$, and $d = 8$) produced smaller crystals of $138 \pm 1 \text{ nm}$ size, as shown in Figure 2c,d (denoted as S/Au). In addition, the crystal surface of S/Au was rougher than that of L/Au (Figure 2b,d, insets). This may be due to the difference in crystallization kinetics: the slow crystallization of L/Au leads to a smooth surface.

The infrared reflection–absorption spectra (IRRAS) of both modified electrodes correspond to that of $[\text{Cu}_3(\text{btc})_2]_n$ synthesized in bulk (SI, Figure S1). X-ray diffraction (XRD) measurements revealed that the larger crystals (L/Au) gave relatively strong $h00$ diffraction intensity, indicating preferential $[100]$ crystal orientation of $[\text{Cu}_3(\text{btc})_2]_n$, but not for the smaller crystals (SI, Figure S2). Although we also used a modified electrode with carboxylic acid-terminated self-assembled monolayers as a supporting substrate, no clear improvement in coverage or orientation was observed. Therefore, we used bare gold substrates for the QCM measurement described below.

In order to clarify the sorption properties of the PCP hybrid, we developed an environment-controlled QCM system, in which the partial vapor pressure of volatile organic compounds (VOCs)

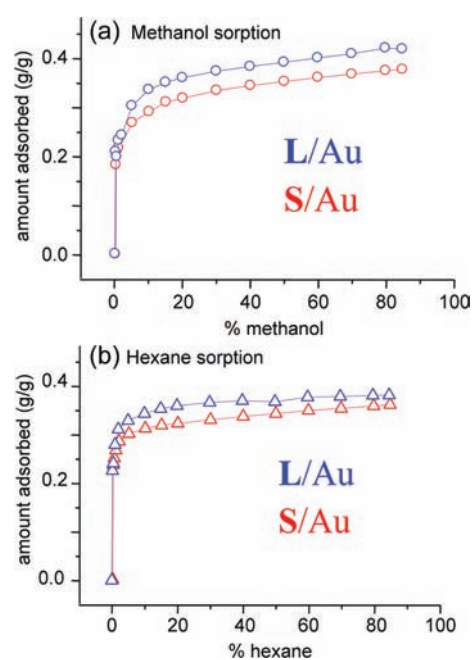


Figure 3. Adsorption isotherms of $[\text{Cu}_3(\text{btc})_2]_n$ nanocrystals on quartz oscillator (L/Au (blue) and S/Au (red)) at 298 K for (a) methanol and (b) hexane.

in helium carrier gas is adjusted by mass flow controllers in the range from 0 to 85% at 298 K with a total mass flow of $100 \text{ cm}^3 \cdot \text{min}^{-1}$ (SI, Figure S3). The PCP-modified QCM substrate (AT-cut, 9 MHz) was activated prior to the measurement according to the following protocol: The modified QCM oscillator was soaked in pure methanol for $>2 \text{ h}$ and then heated at 353 K for 2 h in the QCM chamber under dry helium gas flow. The amount of $[\text{Cu}_3(\text{btc})_2]_n$ nanocrystals deposited on the QCM substrate was estimated at $42.3 \mu\text{g} \cdot \text{cm}^{-2}$ for L/Au and $17.0 \mu\text{g} \cdot \text{cm}^{-2}$ for S/Au (for the details about the conversion of frequency to mass, see SI).

The adsorption isotherms of both L/Au and S/Au at 298 K for methanol and hexane in the range of $P/P_0 = 0\text{--}0.85$ were successfully obtained for the QCM system and presented typical type I sorption profiles (Figure 3). As expected, the saturated adsorption amounts on both L/Au and S/Au at $P/P_0 = 0.85$ were close to each other: methanol uptake was 0.41 and 0.38 g/g, respectively, and hexane uptake was 0.38 and 0.36 g/g, respectively. These values are relatively smaller than those obtained by volumetric sorption measurements for bulk samples (SI, Figure S4). This is most likely due to the difference in the activation methods between the hybrid material and the bulk sample (403 K, 12 h under reduced pressure).

The vapor adsorption kinetics were investigated by real-time monitoring of the frequency change (1 Hz sampling rate) after the introduction of a vapor flow of VOCs into the QCM chamber at both $P/P_0 = 0.002$ (0.2% at the low concentration before saturation) and 0.85 (85% at the high concentration). The time-dependent mass uptakes (M_t/M_e , where M_t is the uptake at time t and M_e is the equilibrium uptake at each concentration) for methanol and hexane vapors on the L/Au and S/Au samples are illustrated in Figure 4 for the low-concentration dosing and in Figure 5 for the high-concentration dosing.

At the low-concentration dosing at $P/P_0 = 0.002$ (Figure 4), we clearly observed a dependence on crystal size for both

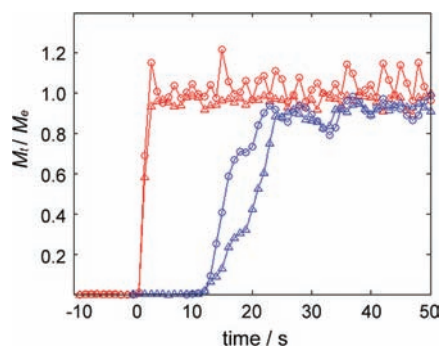


Figure 4. Time-dependent mass uptakes of $[\text{Cu}_3(\text{btc})_2]_n$ nanocrystals on quartz oscillator (L/Au (blue) and S/Au (red)) at low concentration dosing of analytes ($P/P_0 = 0.002$) at 298 K for methanol (O) and hexane (Δ). An offset of 10 s is applied to the data of L/Au for clarity.

methanol and hexane adsorptions. The adsorption uptake of the small crystal sample, S/Au, became saturated in a few seconds. In contrast, it took >10 s to reach saturation for the large crystal sample of L/Au. Note that the step-like structures observed for L/Au are most likely due to the instability of the mass flow controller at the lowest limit of mass flow ($0.2 \text{ cm}^3 \cdot \text{min}^{-1}$), as oscillation was observed even after saturation.

Interestingly, the crystal size rather than the analytes themselves influenced the characteristic rate of mass uptake, which is controlled only by diffusion, defined as D/r^2 (where D is the diffusion coefficient and r is the diffusion length). At such a low concentration, the analyte molecules freely diffuse inside the pores, and there is no interaction between molecules. Therefore, the factor r is significantly pronounced in this condition, and we observed the clear dependence of the sorption uptake on size. Note that the faster uptake of methanol than hexane for L/Au could be related to the larger diffusion coefficient.

At the high concentration dosing at $P/P_0 = 0.85$ (Figure 5), we clearly observed a dependence on the analyte. In the case of methanol, the uptake rates for both S/Au and L/Au are very fast and comparable to one another (Figure 5a). The reason for this fast uptake even in the case of L/Au is still unclear, but one plausible explanation is the following: In the adsorption isotherm of methanol (Figure S4), one can see a step in the region of relative pressures $P/P_0 = 0.05 - 0.10$, which could indicate a cooperative adsorption phenomenon. A similar phenomenon was observed in MOF-5 for carbon dioxide adsorption.¹⁸ This positive cooperative effect of methanol aggregation could explain the faster uptake rate at higher concentration dosing. The detailed mechanism of this cooperative effect is currently under investigation.

The dependence of the sorption kinetics on crystal size for hexane was more emphasized at the high-concentration dosing (Figure 5b). Compared to the uptake rates at the low-concentration dosing, the adsorption kinetics of L/Au became much slower. The time scale over which the mass uptake changed allowed us to fit by physical models, whereas all other uptakes were too fast to follow with sufficient resolution due to the limitation of sampling rate.

Intrinsically, there are two significant processes in the adsorption kinetics of microporous materials: (a) diffusion along the pores and (b) diffusion through the barrier at the pore entrance.¹⁹ Here we compared the prediction of two simple linear models of sorption commonly used in the literature with our experimental results: Model 1, the constant surface concentration model, also known as the Fickian model,²⁰ that only considers the contribution from (a),

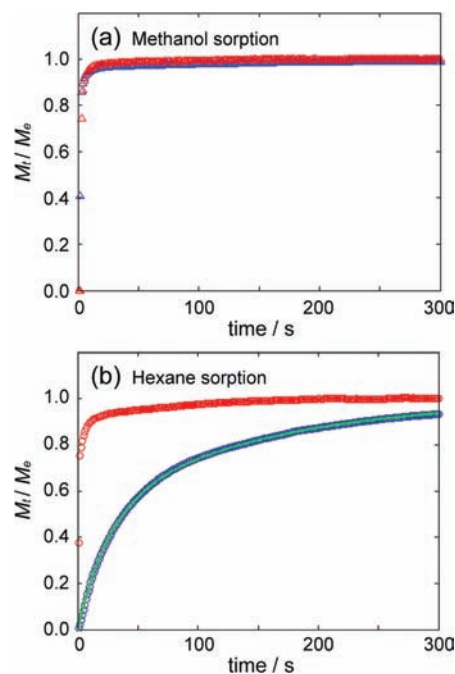


Figure 5. Time-dependent mass uptakes of $[\text{Cu}_3(\text{btc})_2]_n$ nanocrystals on quartz oscillator (L/Au (blue) and S/Au (red)) at high concentration dosing of analytes ($P/P_0 = 0.85$) at 298 K for (a) methanol and (b) hexane. The green line in (b) shows how a constant plus two exponentials fit the L/Au data.

and Model 2, the constant influx and barrier resistance model, also known as the combined barrier resistance and diffusion model,²¹ that includes contributions from both (a) and (b). The predictions of these models are summarized in the SI. Interestingly, neither model gave a satisfactory fit for the normalized experimental data of L/Au, as shown in SI Figure S5 (Model 1, $D/r^2 = 8.0 \times 10^{-4} \text{ s}^{-1}$, with regression coefficient $R^2 = 0.985$; Model 2, $D/r^2 = 9.2 \times 10^{-4} \text{ s}^{-1}$, with $R^2 = 0.989$). One of the shortcomings of these models is their linear nature; the concentration dependence of the diffusion coefficient is neglected. The discrepancy between the experimental data and the prediction of these models is most likely due to the nonlinearity.

Examining the semilogarithmic plot of the mass uptake versus time suggested that the data could be fit by a sum of exponentials. After performing a multiexponential fit, we found that a constant plus two exponentials described the data best, as shown in Figure 5b:

$$M_t/M_e = 1 - A_1 \exp(-k_1 t) - A_2 \exp(-k_2 t) \quad (1)$$

where k_1 and k_2 are kinetic rate constants and A_1 and A_2 are the relative contribution of each rate. The parameters for this fit are found to be $k_1 = (6.55 \pm 0.03) \times 10^{-3} \text{ s}^{-1}$, $k_2 = (3.75 \pm 0.03) \times 10^{-2} \text{ s}^{-1}$, $A_1 = 0.473 \pm 0.003$, $A_2 = 0.544 \pm 0.003$, and $R^2 = 0.9999$. Even though we do not fully understand the nature of the nonlinearity, it most likely introduces an additional time scale (or modifies the weight of existing ones) through a new exponential term that is absent in the linear models.²²

At the low-concentration dosing of analytes (the case of high sensitivity), the sorption kinetics, and thus the sensor response, depended on the crystal size. We prove that the smaller crystal size was appropriate to obtain the faster sensor response, which was independent of the analyte species. Improved

instrumentation will allow us to follow even this very fast kinetics and to quantitatively analyze the diffusion kinetics. In contrast, the high-concentration dosing experiments suggested the importance of sorbate–sorbate interactions in addition to sorbate–framework interactions for understanding the diffusion kinetics.

In this Communication, we have reported the successful synthesis of $[\text{Cu}_3(\text{btc})_2]_n$ nanocrystals on gold-coated QCM substrate at room temperature with fine-tuning of their crystal sizes by coordination modulation method and characterization by AFM, IRRAS, and XRD experiments. By means of an environment-controlled QCM system that can control the relative vapor pressure of VOCs in the QCM chamber, we have studied the sorption kinetics of PCP nanocrystalline films, and our results highlight that downsizing the crystals leads to a faster sensor response at the low-concentration dosing of analytes. These results open the way for the fabrication of not only novel PCP sensor devices with improved sensing performance but also new systems to quantitatively investigate sorption kinetics, which is a significant aspect of molecular separation and catalysis. Further investigations using different PCPs, including SUR-MOFs fabricated by the layer-by-layer method and heterostructured PCPs, as well as the improvement of the environment-controlled QCM system, are currently in progress.

■ ASSOCIATED CONTENT

Supporting Information. IR spectra, XRD patterns, environment-controlled QCM system, volumetric sorption measurements for bulk samples, physical models fitting for hexane sorption kinetics, and complete ref 13c. This material is available free of charge via the Internet at <http://pubs.acs.org>.

■ AUTHOR INFORMATION

Corresponding Author

shuhei.furukawa@icems.kyoto-u.ac.jp; kitagawa@sbchem.kyoto-u.ac.jp

■ ACKNOWLEDGMENT

The authors are grateful to Dr. Kazuyuki Nakai (BEL Japan, Inc.) for assistance in the development of environment-controlled QCM system. The authors are also grateful to Dr. Daisuke Tanaka and Prof. Minoru Miyahara for helpful discussions. M.T. is grateful to the DAAD for a postdoctoral fellowship.

■ REFERENCES

- (1) Yaghi, O. M.; O'Keeffe, M.; Ockwig, N. W.; Chae, H. K.; Eddaoudi, M.; Kim, J. *Nature* **2003**, *423*, 705–714.
- (2) Kitagawa, S.; Kitaura, R.; Noro, S. *Angew. Chem., Int. Ed.* **2004**, *43*, 2334–2375.
- (3) Férey, G.; Mellot-Draznieks, C.; Serre, C.; Millange, F. *Acc. Chem. Res.* **2005**, *38*, 217–225.
- (4) Dincá, M.; Long, J. R. *Angew. Chem., Int. Ed.* **2008**, *47*, 6766–6779.
- (5) Morris, R. E.; Wheatley, P. S. *Angew. Chem., Int. Ed.* **2008**, *47*, 4966–4981.
- (6) Wang, Z.; Cohen, S. M. *Chem. Soc. Rev.* **2009**, *38*, 1315–1329.
- (7) Perry, J. J., IV; Perman, J. A.; Zaworotko, M. J. *Chem. Soc. Rev.* **2009**, *38*, 1400–1417.
- (8) Shimizu, G. K.; Vaidhyanathan, R.; Taylor, J. M. *Chem. Soc. Rev.* **2009**, *38*, 1430–1449.

- (9) Lee, J. Y.; Farha, O. K.; Roberts, J.; Scheidt, K. A.; Nguyen, S. T.; Hupp, J. T. *Chem. Soc. Rev.* **2009**, *38*, 1450–1459.
- (10) Li, J. R.; Kuppler, R. J.; Zhou, H.-C. *Chem. Soc. Rev.* **2009**, *38*, 1477–1504.
- (11) Biemmi, E.; Darga, A.; Stock, N.; Bein, T. *Microporous Mesoporous Mater.* **2008**, *114*, 380–386.
- (12) Zybaylo, O.; Shekhah, O.; Wang, H.; Tafipolsky, M.; Schmid, R.; Johannsmann, D.; Wöll, C. *Phys. Chem. Chem. Phys.* **2010**, *12*, 8092–8097.
- (13) (a) Lin, W.; Rieter, W.; Taylor, K. *Angew. Chem., Int. Ed.* **2009**, *48*, 650–658. (b) Spokoyny, A. M.; Kim, D.; Sumrein, A.; Mirkin, C. A. *Chem. Soc. Rev.* **2009**, *38*, 1218–1227. (c) Horcajada, P.; et al. *Nat. Mater.* **2009**, *9*, 172–178. (d) Tanaka, D.; Henke, A.; Albrecht, K.; Moeller, M.; Nakagawa, K.; Kitagawa, S.; Groll, J. *Nature Chem.* **2010**, *2*, 410–416.
- (14) (a) Zacher, D.; Shekhah, O.; Wöll, C.; Fischer, R. A. *Chem. Soc. Rev.* **2009**, *38*, 1418–1430. (b) Hermes, S.; Schröder, F.; Chelmoski, R.; Wöll, C.; Fischer, R. A. *J. Am. Chem. Soc.* **2005**, *127*, 13744–13745. (c) Biemmi, E.; Scherb, C.; Bein, T. *J. Am. Chem. Soc.* **2007**, *129*, 8054–8055. (d) Shekhah, O.; Wang, H.; Kowarik, S.; Schreiber, F.; Paulus, M.; Tolan, M.; Sternemann, S.; Evers, F.; Zacher, D.; Fischer, R. A.; Wöll, C. *J. Am. Chem. Soc.* **2007**, *129*, 15118–15119. (e) Gascon, J.; Aguado, S.; Kapteijn, F. *Microporous Mesoporous Mater.* **2008**, *113*, 132–138. (f) Ameloot, R.; Gobechiya, E.; Uji-i, H.; Martens, J. A.; Hofkens, J.; Alaerts, L.; Sels, B. F.; De Vos, D. E. *Adv. Mater.* **2010**, *22*, 2685–2688. (g) Makiura, R.; Motoyama, S.; Umamura, Y.; Yamanaka, H.; Sakata, O.; Kitagawa, H. *Nat. Mater.* **2010**, *9*, 565–571.
- (15) (a) Allendorf, M. D.; Houk, R. J. T.; Andruszkiewicz, L.; Talin, A. A.; Pikarsky, J.; Choudhury, A.; Gall, K. A.; Hesketh, P. J. *J. Am. Chem. Soc.* **2008**, *130*, 14404–14405. (b) Guo, H.; Zhu, G.; Hewitt, I. J.; Qiu, S. *J. Am. Chem. Soc.* **2009**, *131*, 1646–1647. (c) Horcajada, P.; Serre, C.; Grosso, D.; Boissière, C.; Perruchas, S.; Sanchez, C.; Férey, G. *Adv. Mater.* **2009**, *21*, 1931–1935. (d) Bae, Y.-S.; Spokoyny, A. M.; Farha, O. K.; Snurr, R. Q.; Hupp, J. T.; Mirkin, C. A. *Chem. Commun.* **2010**, *46*, 3478–3480. (e) Lu, G.; Hupp, J. T. *J. Am. Chem. Soc.* **2010**, *132*, 7832–7833.
- (16) Tsuruoka, T.; Furukawa, S.; Takashima, Y.; Yoshida, K.; Isoda, S.; Kitagawa, S. *Angew. Chem., Int. Ed.* **2009**, *48*, 4739–4743.
- (17) Diring, S.; Furukawa, S.; Takashima, Y.; Tsuruoka, T.; Kitagawa, S. *Chem. Mater.* **2010**, *22*, 4531–4538.
- (18) Walton, K. S.; Millward, A. R.; Dubbeldam, D.; Frost, H.; Low, J. J.; Yaghi, O. M.; Snurr, R. Q. *J. Am. Chem. Soc.* **2008**, *130*, 406–407.
- (19) (a) Rao, M. B.; Jenkins, R. G.; Steele, W. A. *Langmuir* **1985**, *1*, 137–141. (b) Reid, C. R.; Thomas, K. M. *Langmuir* **1999**, *15*, 3206–3218. (c) Fletcher, A. J.; Cussen, E. J.; Prior, T. J.; Rosseinsky, M. J.; Kepert, C. J.; Thomas, M. K. *J. Am. Chem. Soc.* **2001**, *123*, 10001–10011. (d) Fletcher, A. J.; Cussen, E. J.; Bradshaw, D.; Rosseinsky, M. J.; Thomas, K. M. *J. Am. Chem. Soc.* **2004**, *126*, 9750–9759.
- (20) Foley, N. J.; Thomas, K. M.; Forshaw, P. L.; Stanton, D.; Norman, P. R. *Langmuir* **1997**, *13*, 2083–2089.
- (21) Loughlin, K. F.; Hassan, M. M.; Fatehi, A. I.; Zahur, M. *Gas Sep. Purif.* **1993**, *7*, 264–273.
- (22) In some simple cases, such as desorption from a slab of a certain thickness, the effect of nonlinearity in the form of a concentration-dependent diffusion coefficient can be well approximated at sufficiently long times by including additional exponentials in the linear model. See, for example: (a) Crank, J. *The Mathematics of Diffusion*; Oxford University Press: New York, 1975; pp 104–136. (b) Tsang, T. J. *Appl. Phys.* **1961**, *32*, 1518–1520.
- (23) Tanaka, D.; Nakagawa, K.; Higuchi, M.; Horike, S.; Kubota, Y.; Kobayashi, T. C.; Takata, M.; Kitagawa, S. *Angew. Chem., Int. Ed.* **2008**, *47*, 3914–3918.
- (24) Chmelik, C.; Kärger, J.; Wiebcke, M.; Caro, J.; van Baten, J. M.; Krishna, R. *Microporous Mesoporous Mater.* **2009**, *117*, 22–32.
- (25) Berenguer-Murcia, A.; Fletcher, A. J.; Garcia-Martinez, J.; Cazorla-Amorós, D.; Linares-Solano, A.; Thomas, K. M. *J. Phys. Chem. B* **2003**, *107*, 1012–1020.